Infrared study of the charge-ordered multiferroic LuFe$_2$O$_4$

F. M. Vitucci,[1,2] A. Nucara,[1] D. Nicoletti,[1] Y. Sun,[3] C. H. Li,[3] J. C. Soret,[2] U. Schade,[4] and P. Calvani[1]

[1]*CNR-SPIN and Dipartimento di Fisica, Università di Roma La Sapienza, Piazzale A. Moro 2, I-00185 Roma, Italy*

[2]*LEMA-CNRS, Université de Tours, F-37200 Tours, France*

[3]*Beijing National Laboratory for Condensed Matter Physics, Institute of Physics, Chinese Academy of Sciences, Beijing 100080, People's Republic of China*

[4]*Berliner Elektronenspeicherring-Gesellschaft für Synchrotronstrahlung m.b.H., Albert-Einstein Strasse 15, D-12489 Berlin, Germany*

The reflectivity of a large LuFe$_2$O$_4$ single crystal has been measured with the radiation field either perpendicular or parallel to the c axis of its rhombohedral structure, from 10 to 500 K, and from 7 to 16 000 cm^{-1}. The transition between the two-dimensional and the three-dimensional charge order at T_{CO}=320 K is found to change dramatically the phonon spectrum in both polarizations. The number of the observed modes above and below T_{CO}, according to a factor-group analysis, is in good agreement with a transition from the rhombohedral space group $R\bar{3}m$ to the monoclinic $C2/m$. In the subteraahertz region a peak becomes evident at low temperature, whose origin is discussed in relation with previous experiments.

I. INTRODUCTION

The multiferroics are materials which exhibit, in a common range of temperatures, both ferroelectricity and magnetic order (ferromagnetism, ferrimagnetism or antiferromagnetism). Much effort has been devoted to understand the relationship between their magnetic and electronic degrees of freedom,[1–3] in view of the potential applications. Indeed, the conventional mechanisms of ferroelectricity and magnetism are not compatible with each other, and this makes the multiferroic materials relatively rare. One should then invoke novel mechanisms of ferroelectricity, as those associated with specific charge configurations in charge-ordered materials.[4] One of such compounds is the mixed-valence LuFe$_2$O$_4$ (LFO). Its structure belongs to the rhombohedral space group $R\bar{3}m$ and includes triangular double layers of Fe-O stacked along the c axis. A two-dimensional Fe^{2+}/Fe^{3+} charge order (CO), which forms between about 500 K and T_{CO}=320 K in those double layers, builds up in each Fe-O plane a net dipole moment.[5–7] Below T_{CO}, the CO becomes more robust and three-dimensional (3D).

Dielectric measurements in low electric fields show that the 3D phase of LFO is ferroelectric,[7] while x-ray scattering indicates that the dipole moments of adjacent bilayers are antiparallel,[8] so that the net polarization is zero. These contradictory findings can be reconciled by considering that the antiferroelectric ground state and the ferroelectric state may be so close in energy[8] that even a small electric field stabilizes the latter one. Concerning the magnetic behavior of LFO, a two-dimensional ferrimagnetic order is established below $T_N \simeq 240$ K.[9] However, a surprising decrease in the magnetic correlation length is observed below T_L=175 K.[10] Finally, it has been found that the dielectric constant decreases sharply both under weak magnetic[11] and electric[12] fields, which also cause a drop in the resistivity by several orders of magnitude.[13] This colossal electroresistance, which is also observed at room temperature, makes LFO attractive for its potential applications.

The optical response of LFO with the radiation field $\mathbf{E} \perp \mathbf{c}$ has been investigated by Xu *et al.*,[14] together with other

properties, between 30 and 6.5 eV and from 4 to 540 K. At zero field the authors observe two main peaks in the near-infrared and visible range, which is dominated by electronic excitations. The band at 1.1 eV is assigned to Fe^{2+}/Fe^{3+} charge transfer, and that at about 3.5 eV to a superposition of O$-p \rightarrow$Fe-d and O$-p \rightarrow$Lu$-s$ charge transfer. The edge of the 1.1 eV peak creates the insulating optical gap at ∼0.5 eV. A third feature in the midinfrared, peaked at about 0.3 eV, is attributed by the authors to on-site Fe^{3+} excitations. Li *et al.*[15] have instead explored the subteraahertz response of LFO by time-domain spectroscopy, observing at low T two collective excitations that they assigned to a central mode and to a soft mode of the ferroelectric phase.

In the present experiment we have investigated both the subteraahertz and the infrared optical conductivity of LuFe$_2$O$_4$ by Fourier-Transform spectroscopy. We performed reflectivity measurements on a large single crystal from 7 to 16 000 cm^{-1} (i.e., from about 1 to 2 eV), in the temperature range 10–500 K, with the radiation field $\mathbf{E}$ polarized both $\perp \mathbf{c}$ and $\|\mathbf{c}$. We could thus observe in detail the optical-phonon spectrum of LuFe$_2$O$_4$, and the striking modifications that it undergoes when crossing T_{CO}. In the subteraahertz spectral range we detected at low T a peak at 10 cm^{-1}, which corresponds approximately to the central mode reported in Ref. 15. We propose for that spectral feature an alternative interpretation which is related to charge order rather than to ferroelectricity.

II. EXPERIMENT

The measurements were performed on a large ($8 \times 3 \times 2$ mm^3) single crystal of LuFe$_2$O$_4$, grown by optical floating zone melting method in a flowing argon atmosphere,[16] and characterized by x-ray diffraction and Laue imaging at room temperature. The magnetic susceptibility of the sample, as measured in zero-fied cooling, is shown in Fig. 1. In addition to the sharp peak at T_N=230 K, also reported previously,[15] we observe a change of slope at about 150 K which may be related to the change in the magnetic correla-
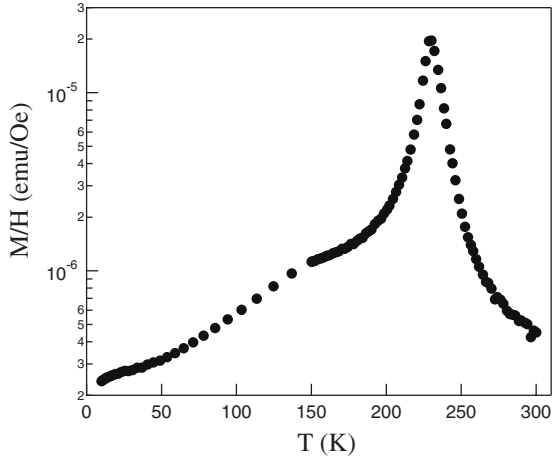
FIG. 1. Magnetic susceptibility of the single crystal of $LuFe_2O_4$, as measured in zero-field cooling.

tion length observed in neutron scattering experiments around 175 K.

The largest crystal surface contained the axes *c* and *a* (or *b*). Its reflectivity $R(\omega)$ was measured between 7 and 16 000 cm^{-1} by Michelson interferometers, with the radiation field **E** polarized either $\perp$**c** or $\parallel$**c**. Below 300 K the sample was thermoregulated within ± 2 K in a He-flow cryostat, above 300 K in an evacuated capsule and in thermal contact with a heater. Both sample holders included a mobile hot filament for gold evaporation. Indeed, after measuring the intensity $I_s(\omega)$ reflected by the sample, at each temperature gold was evaporated *in situ*, and the intensity $I_0(\omega)$ reflected by the golden sample was measured for reference. The reflectivity $R(\omega) = I_s(\omega)/I_0(\omega)$ was thus obtained. The subterahertz measurements were performed by the same procedure but using the coherent synchrotron radiation extracted from a bending magnet of the BESSY-II storage ring when working in its low-α mode.[17] The real part of the optical conductivity was calculated by the use of Kramers-Kronig transformations. Standard extrapolations were applied to $R(\omega)$ at all temperatures, at frequencies both lower and higher than the measured interval.

III. RESULTS AND DISCUSSION

A. Reflectivity and high-frequency conductivity

The reflectivity of the LFO crystal is reported in Fig. 2 for **E** $\perp$ **c** (a) and **E**$\parallel$**c** (b). In both panels $R(\omega)$ shows a rich and detailed optical-phonon spectrum, also reported on a linear scale in the insets, which changes drastically at T_{CO}. In the **E** $\perp$ **c** configuration, at the lowest frequency and high *T*, the nonzero slope of $R(\omega)$ reveals a small and narrow Drude-like term, thermally activated. Below T_{CO}, in the subterahertz region one instead detects a weak but well defined peak at about 10 cm^{-1}. The mid- and the near-infrared ranges are finally occupied by a broad, practically *T*-independent band with a maximum around 8000 cm^{-1} (1 eV).

This broad peak is better seen in Fig. 3, which shows the real part of the optical conductivity, as extracted from $R(\omega)$ by the Kramers-Kronig transformations. The figure reports
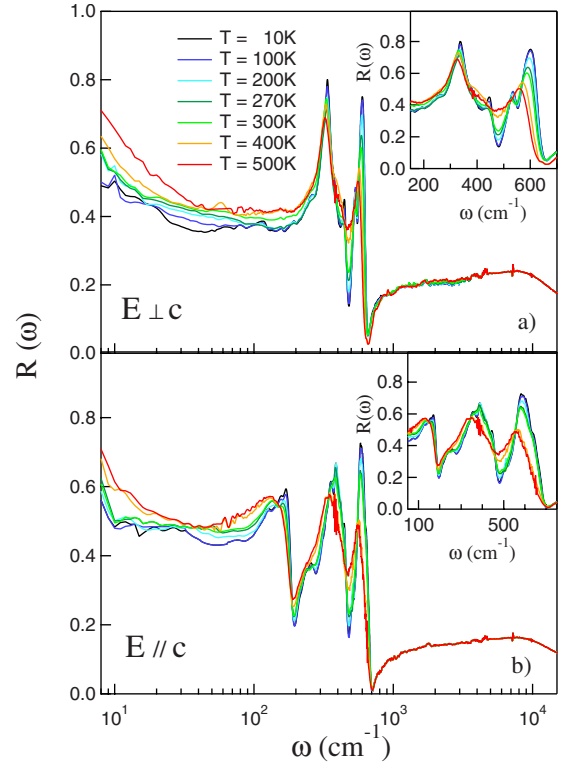

FIG. 2. (Color online) Reflectivity of $LuFe_2O_4$ between 10 and 500 K, as measured with the radiation field polarized along the $a(b)$ axis (above) and along the *c* axis (below). The phonon region is reported in the inset on a linear frequency scale.

the data at 10 K, but the high-frequency conductivity is virtually independent of temperature. The best fit, also plotted in the figure, requires a strong oscillator peaked at 7200 cm^{-1} (0.9 eV) for **E** $\perp$ **c** and at 8400 cm^{-1} (1.05 eV) for **E**$\parallel$**c**. The former one is in fair agreement with the contribution at 1.1 eV reported in Ref. 14 and assigned to the
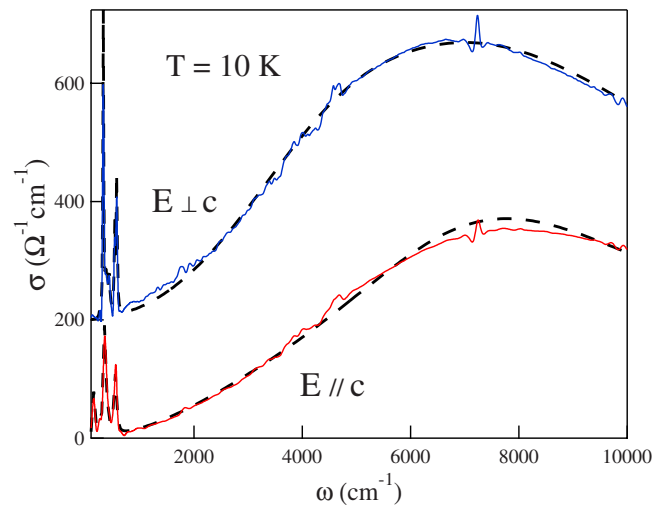

FIG. 3. (Color online) Optical conductivity of $LuFe_2O_4$ at 10 K in the whole energy range, as measured with the radiation field **E** $\perp$ **c** or **E**$\parallel$**c**. The fitting curves are reported by dashed lines. The zero of the upper curves has been shifted by 200 Ω^{-1} cm^{-1} for sake of clarity.

TABLE I. Site symmetries of the seven atoms per formula unit, and irreducible representations of the vibrational modes, in the rhombohedral unit cell $R\bar{3}m$ of $LuFe_2O_4$.

Atoms	Wyckoff notation	Site symmetry	Irreducible representation
Fe, Fe	1(a), 1(b)	D_{3d}	$2E_u+2A_{2u}$
Lu,O	2(c)	C_{3v}	$E_g+E_u+A_{1g}+A_{2u}$
O,O,O	3(d)	C_{2h}	$3E_u+A_{1u}+2A_{2u}$

lowest-energy allowed electronic transition,[18] namely, the $Fe^{2+}\rightarrow Fe^{3+}$ charge transfer. This may occur between one of the doubly degenerate E levels, which slightly differ in energy from each other, and the A-symmetry singlet at higher energy.[19]

The authors of Ref. 14 also report a much weaker contribution at 0.3 eV, detected in transmission measurements on thin samples. They assign it to on-site Fe^{3+} excitations, but it might also be due to the photoionization of the polaronic charges in the CO state.[20] Indeed, the mobility of the charges in the CO regime is treated in Ref. 14 in terms of small-polaron hopping. In the present reflectivity spectra we do observe a weak, lower-energy sideband of the main peak, that however the fit places (at 10 K) at 4000 cm^{-1} (0.5 eV) for $\mathbf{E}\perp\mathbf{c}$ and at 4500 cm^{-1} (0.55 eV) for $\mathbf{E}\|\mathbf{c}$.

B. Optical conductivity in the phonon region

The high-temperature, rhombohedral $R\bar{3}m$ unit cell of $LuFe_2O_4$ contains 3 f.u., rotated by 120° around $\mathbf{c}$ with respect to one another, having the same 3 acoustic and 18 optical modes. The authors of Ref. 21 assumed $3E_u$ and $3E_g$ (doubly degenerate) optical phonons in the ab plane, $3A_{2u}$ and $3A_{1g}$ (nondegenerate) optical modes for the c axis, and calculated their frequencies (the u modes are infrared active, the g's are Raman active). However, a factor-group analysis[22] leads us to a more complex phonon scenario for $LuFe_2O_4$, as it is shown in Table I.

The resulting modes are classified in Table II with respect to their polarization and activity. In the high-T $R\bar{3}m$ symmetry, the infrared-active modes are predicted to be $5E_u$ in the ab plane, $4A_{2u}$ along the c axis. At low T, the CO reduces the crystal symmetry to the monoclinic $C2/m$,[8] which includes one site of symmetry $C_{2h}(1)$, two $C_i(2)$, two $C_2(2)$, and two $C_s(2)$. Here, the number in parenthesis indicates how many atoms each site can accommodate. One thus obtains eight

TABLE II. Classification of the phonon modes predicted for the ab plane and the c axis, in the $R\bar{3}m$ high-temperature phase of $LuFe_2O_4$.

	Infrared active	Raman active	Acoustic	Silent
ab plane	$5E_u$	E_g	E_u	
c axis	$4A_{2u}$	A_{1g}	A_{2u}	A_{1u}

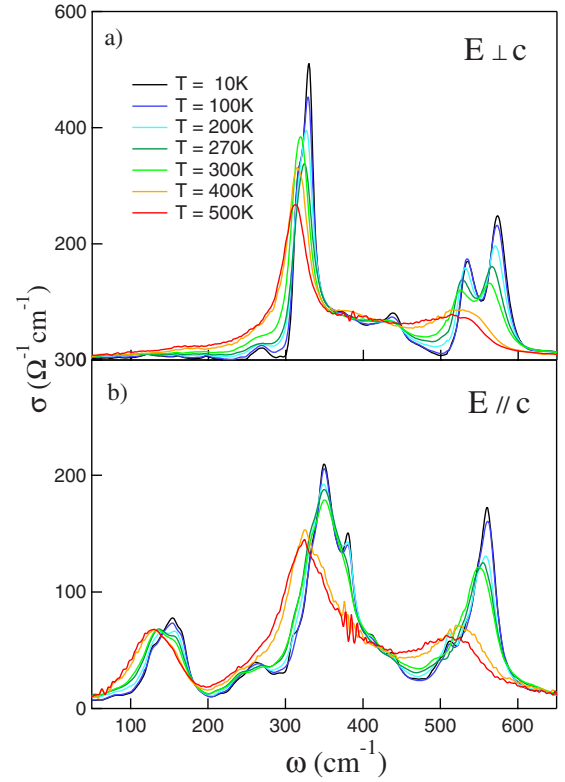FIG. 4. (Color online) Optical conductivity of $LuFe_2O_4$ between 10 and 500 K in the phonon region, as measured with the radiation field $\mathbf{E}\perp\mathbf{c}$ and $\mathbf{E}\|\mathbf{c}$.

possible irreducible representations Γ_i, depending on the site occupation. The Γ_i's with $i=1,\dots,4$ lead to 12 one-dimensional infrared-active modes, those with $i=5,\dots,8$ to 15 such modes. However, six out of them require that a site with inversion symmetry C_i is occupied. As such an atom does not exist even in the high-T phase, they can all be excluded. The remaining two irreducible representations of the crystal vibrations, in the low-T $C2/m$ phase, are

$$\Gamma_1 = 4A_u + 8B_u + 2A_g + 4B_g,$$

$$\Gamma_2 = 4A_u + 8B_u + 3A_g + 3B_g. \tag{1}$$

They differ for the Raman spectrum but predict the same 12 infrared-active, nondegenerate, modes. One thus obtains a reliable prediction on the effect of the symmetry reduction below T_{CO} on the phonon spectrum.

This effect is clearly seen in Fig. 4, which shows the optical conductivity of LFO measured in the far infrared. Below 320 K, for $\mathbf{E}\perp\mathbf{c}$ the broad contribution at 530 cm^{-1} splits into two components separated by about 40 cm^{-1}; for $\mathbf{E}\|\mathbf{c}$ all lines shift abruptly to higher frequencies and new components do appear. Incidentally, no phonon line displays Fano-like asymmetries,[23] thus confirming the absence of a free-carrier background in the phonon energy range.

In order to obtain a closer comparison with theory, the optical conductivity was fit, through the relation $\sigma = (\omega/4\pi)\epsilon_2$, to the imaginary part ϵ_2 of the Lorentzian dielectric function
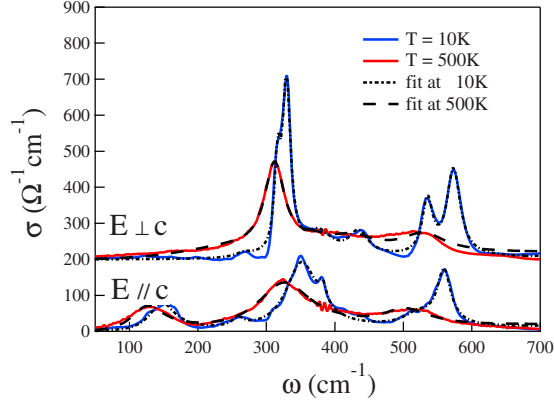
FIG. 5. (Color online) Optical conductivity at 10 and 500 K, for both $\mathbf{E} \perp \mathbf{c}$ and $\mathbf{E} \| \mathbf{c}$, with the fitting curves which provide the parameters listed in Table III. The zero of the upper curves has been shifted by 200 Ω^{-1} cm^{-1} for sake of clarity.

$$\widetilde{\epsilon}(\omega) = \epsilon_1 + i\epsilon_2 = \epsilon_\infty + \sum_{j=1}^{n} \frac{A_j \Omega_{TO_j}^2}{\Omega_{TO_j}^2 - \omega^2 - i\gamma_j \omega}. \quad (2)$$

Therein, ϵ_∞ accounts for the high-frequency contributions to $\widetilde{\epsilon}(\omega)$, while Ω_{TO_j}, A_j and γ_j are the central frequency, strength and damping of the jth mode, respectively. The accuracy of the procedure can be evaluated in Fig. 5, where the fitting curves are compared with the experimental $\sigma(\omega)$ at both extreme temperatures.

The parameters obtained by fitting Eq. (2) to the optical conductivity of Fig. 4 with the minimum possible number of oscillators, both in the rhombohedral $R\bar{3}m$ cell at 500 K, and in the monoclinic $C2/m$ cell at 10 K, are listed in Table III. Therein, a good agreement with the factor-group predictions reported in Table II and in Eq. (1) is displayed. At high T one obtains a good fit by using five Lorentzians in the ab plane, three along the c axis, to be compared with the five and four infrared modes, respectively, predicted in Table II. At low T, in the monoclinic symmetry, the best fit requires six modes for $\mathbf{E} \perp \mathbf{c}$ and six for $\mathbf{E} \| \mathbf{c}$, in excellent agreement with the 12 infrared-active phonons predicted in total by Eq. (1). A shoulder which appears at 316 cm^{-1} both for $\mathbf{E} \perp \mathbf{c}$ and $\mathbf{E} \| \mathbf{c}$ is unlikely to be due to a normal mode of the crystal.

The temperature evolution of the main phonon frequencies is shown in Fig. 6 for both the ab plane and the c axis. Therein one may clearly see the branching at T_{CO} of the highest-energy mode of the ab plane and of two modes of the c axis. In all these cases, a narrower line originates from the high-T absorption at a moderately higher frequency, while a new mode springs up at a much higher frequency.

C. Optical response in the subterahertz region

As already mentioned, we have extended our investigation well below the phonon region, in the subterahertz range,

TABLE III. Parameters obtained by fitting Eq. (2) to the phonon spectrum of LuFe$_2$O$_4$, as measured with the radiation field polarized in the ab-plane and along the c-axis. The calculated values are those reported in Ref. 21. All figures are in cm^{-1}.

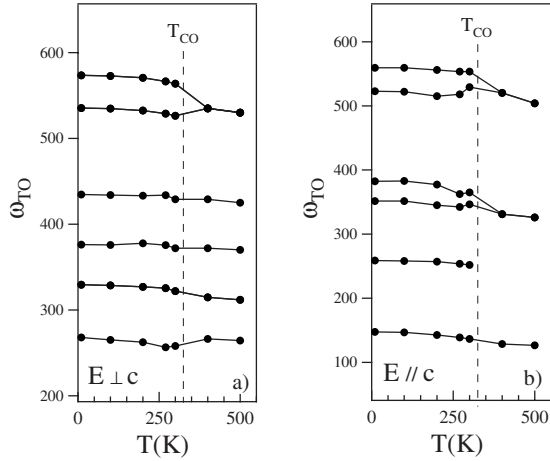| Mode	Ω_{TO}	γ	A	Ω_{calc}	Ω_{TO}	γ	A
				$\mathbf{E} \perp \mathbf{c}$			
		10 K				500 K	
				92			
a1	268	30	150		264	34	190
	316						
a2	329	14	642	332	312	35	700
a3	376	50	441		370	43	215
a4	435	34	361		425	85	441
a5	535	18	408	474	530	75	473
a6	573	23	579				
				$\mathbf{E} \| \mathbf{c}$			
		10 K				500 K	
c1	148	46	461	161	127	59	493
c2	259	22	175				
	316						
c3	352	56	787	310	326	95	856
c4	383	12	196				
c5	523	55	341	465	504	83	466
c6	559	24	467				

FIG. 6. Temperature dependence of the phonon frequencies for $\mathbf{E} \perp \mathbf{c}$ (left) and $\mathbf{E} \| \mathbf{c}$ (right) in LuFe$_2$O$_4$.

FIG. 7. (Color online) Optical conductivity for $\mathbf{E} \perp \mathbf{c}$ of LuFe$_2$O$_4$ in the subterahertz region at different temperatures. The arrows mark the frequencies of the peaks in ϵ_2 extracted from a time-domain experiment (Ref. 15).

by use of coherent synchrotron radiation. We could thus greatly enhance the signal-to-noise ratio on the reflectivity, while maintaining a low perturbation on the system. The $R(\omega)$ thus obtained can be seen in Fig. 2 thanks to its logarithmic frequency scale. Therein, at 100 and 10 K a well defined peak appears at $\omega_0 = 10$ cm^{-1}. This extremely low-frequency feature is then associated with the three-dimensional charge order, further reinforced by the ferrimagnetic transition at 240 K. The resulting subterahertz optical conductivity is reported in Fig. 7, with the feature at ω_0 again evident at low temperature. In Ref. 15, a peak was detected in the ϵ_2 extracted from time-resolved subterahertz spectroscopy.[15] At 50 K it was reported at 13 cm^{-1} (left arrow in Fig. 7), in agreement within errors with the present ω_0. The authors of Ref. 15 attributed their peak to a central mode of the ferroelectric LFO phase. They observed a further, broad contribution around 40 cm^{-1} (right arrow in Fig. 7), which was assigned to a soft mode. In Fig. 7, at 10 K, a second absorption possibly appears between 20 and 30 cm^{-1}.

The present observations may be consistent with those of time-resolved spectroscopy, if one considers that in polycrystalline samples, as is the case of Ref. 15, the soft mode stiffens with respect to that observed in single crystals.[24] However, if one considers that LuFe$_2$O$_4$, as already mentioned, does not exhibit bulk ferroelectricity at zero field, there are alternative explanations for the present peak at 10 cm^{-1} (and for the broad band at higher frequency, if confirmed by further experiments). Indeed, similar features have been observed in several systems where the charge order can be described in terms of charge density waves (CDW) and this is also the case of LFO.[9] For example, in the manganite La$_{0.25}$Ca$_{0.75}$MnO$_3$, below the charge ordering temperature T_{CO} a narrow peak at 7.5 cm^{-1} is observed, followed by a broad absorption at ~ 30 cm^{-1}.[25] The former feature has been interpreted as a collective excitation (phason) of the CDW, which displaces from zero to a finite frequency when either it is pinned to lattice impurities or the charge order is commensurate with the lattice. The broader band was ascribed to a combination band of the phason with the ampli-
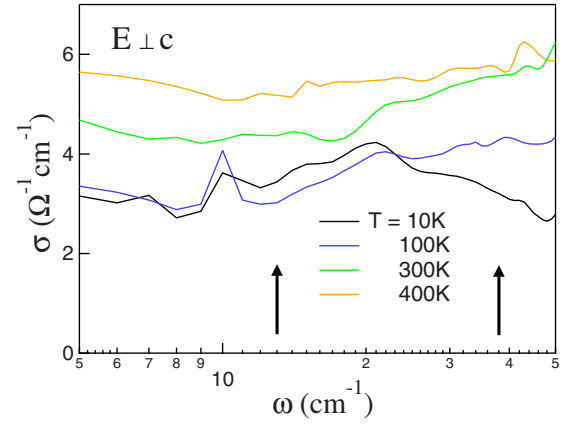
tudon, another excitation which is present in a CDW.[25] According to other authors, the highest-frequency feature is instead due to an acoustic phonon, which becomes infrared active at zero wave vector due to the folding of the Brillouin zone determined by the CO.[26] Further subterahertz experiments are probably needed, before reaching a common interpretation of the elusive excitations which are detected at those low frequencies in the charge-ordered systems.

IV. CONCLUSION

In conclusion, we have reported here a study of the charge-ordered multiferroic LuFe$_2$O$_4$ in the infrared and the subterahertz range, with special focus on the optical-phonon region. Therein we have observed the dramatic effect of the symmetry reduction—caused by the transition at $T_{CO} = 320$ K between the 2D and 3D charge order—both on the modes of the ab plane and on those of the c axis of the rhombohedral structure. Below T_{CO} some phonon bands split into pairs of narrower lines, while new modes do appear. The number of the observed phonon lines, both above and below T_{CO}, is in good agreement with a factor-group analysis of the respective cell symmetries. No evident effects on the phonon spectrum is instead detected when crossing the ferrimagnetic transition at 240 K. In the subterahertz region, a very weak electric conduction, thermally activated, is detected at high temperature, while a peak becomes evident in the low-temperature optical conductivity, possibly accompanied by a broad absorption at higher frequency. For that feature, similar to the one reported previously in time-domain experiments, we have proposed an interpretation related to the charge order rather than to ferroelectricity, and based on a comparison with similar subterahertz spectra recently obtained in charge-ordered manganites at low temperature.

[1] W. Eerenstein, N. D. Mathur, and J. F. Scott, Nature (London) **442**, 759 (2006).

[2] N. A. Spaldin and M. Fiebig, Science **309**, 391 (2005).

[3] N. A. Hill, J. Phys. Chem. B **104**, 6694 (2000).

[4] J. van den Brink and D. I. Khomskii, J. Phys.: Condens. Matter **20**, 434217 (2008).

[5] M. Tanaka, K. Siratori, and N. Kimizuka, J. Phys. Soc. Jpn. **53**, 760 (1984).

[6] N. Ikeda, K. Kohn, N. Myouga, E. Takahashi, H. Kitoh, and S. Takekawa, J. Phys. Soc. Jpn. **69**, 1526 (2000).

[7] N. Ikeda, H. Ohsumi, K. Ohwada, K. Ishii, T. Inami, K. Kakurai, Y. Murakami, K. Yoshii, S. Mori, Y. Horibe, and H. Kito, Nature (London) **436**, 1136 (2005).

[8] M. Angst, R. P. Hermann, A. D. Christianson, M. D. Lumsden, C. Lee, M.-H. Whangbo, J.-W. Kim, P. J. Ryan, S. E. Nagler, W. Tian, R. Jin, B. C. Sales, and D. Mandrus, Phys. Rev. Lett. **101**, 227601 (2008).

[9] Y. Yamada, S. Nohdo, and N. Ikeda, J. Phys. Soc. Jpn. **66**, 3733 (1997); Y. Yamada, K. Kitsuda, S. Nohdo, and N. Ikeda, Phys. Rev. B **62**, 12167 (2000).

[10] A. D. Christianson, M. D. Lumsden, M. Angst, Z. Yamani, W. Tian, R. Jin, E. A. Payzant, S. E. Nagler, B. C. Sales, and D. Mandrus, Phys. Rev. Lett. **100**, 107601 (2008).

[11] M. A. Subramanian, T. He, J. Chen, N. S. Rogado, T. G. Calvarese, and A. W. Sleight, Adv. Mater. (Weinheim, Ger.) **18**, 1737 (2006).

[12] C. Li, X.-Q. Zhang, Z.-H. Cheng, and Y. Sun, Appl. Phys. Lett. **92**, 182903 (2008).

[13] C. Li, X. Zhang, Z. Cheng, and Y. Sun, Appl. Phys. Lett. **93**, 152103 (2008).

[14] X. S. Xu, M. Angst, T. V. Brinzari, R. P. Hermann, J. L. Musfeldt, A. D. Christianson, D. Mandrus, B. C. Sales, S. McGill, J.-W. Kim, and Z. Islam, Phys. Rev. Lett. **101**, 227602 (2008).

[15] S. Z. Li, S. J. Luo, R. Fu, B. B. Jin, K. F. Wang, J.-M. Liu, J. F. Ding, X. G. Li, Appl. Phys. A: Mater. Sci. Process. **96**, 893 (2009).

[16] C. H. Li, F. Wang, Y. Liu, X. Q. Zhang, Z. H. Cheng, and Y. Sun, Phys. Rev. B **79**, 172412 (2009).

[17] M. Abo-Bakr, J. Feikes, K. Holldack, P. Kuske, W. B. Peatman, U. Schade, G. Wüstefeld, and H. W. Hübers, Phys. Rev. Lett. **90**, 094801 (2003).

[18] H. J. Xiang and M.-H. Whangbo, Phys. Rev. Lett. **98**, 246403 (2007).

[19] A. Nagano, M. Naka, J. Nasu, and S. Ishihara, Phys. Rev. Lett. **99**, 217202 (2007).

[20] P. Calvani, Riv. Nuovo Cimento **24**, 1 (2001).

[21] A. B. Harris and T. Yildirim, Phys. Rev. B **81**, 134417 (2010).

[22] G. W. Hateley, F. R. Dollish, N. T. McDevitt, and F. F. Bentley, *Infrared and Raman Selection Rules for Molecular and Lattice Vibrations* (Wiley, New York, 1972).

[23] S. Lupi, M. Capizzi, P. Calvani, B. Ruzicka, P. Maselli, P. Dore, and A. Paolone, Phys. Rev. B **57**, 1248 (1998).

[24] J. Petzelt, J. Hlinka, S. Kamba, T. Ostapchuk, D. Nouijni, and I. Rythchetsky, Ferroelectrics **334**, 199 (2006).

[25] A. Nucara, P. Maselli, P. Calvani, R. Sopracase, M. Ortolani, G. Gruener, M. Cestelli Guidi, U. Schade, and J. García, Phys. Rev. Lett. **101**, 066407 (2008).

[26] T. Zhang, E. Zhukova, B. Gorshunov, D. Wu, A. S. Prokhorov, V. I. Torgashev, E. G. Maksimov, and M. Dressel, Phys. Rev. B **81**, 125132 (2010).